SAE International

Microfluidic Simulation of Diesel Exhaust Gas and Soot Oxidation in Diesel Particulate Filter

2013-01-0009
TSAE-13AP-0009
Published 03/25/2013

Kazuhiro Yamamoto
Nagoya University

Yasunari Hanaki
Nissan Motor Co., Ltd.

doi:10.4271/2013-01-0009

ABSTRACT

Particulate matter (PM) including soot in diesel exhaust gas is a serious atmospheric pollutant, and stricter exhaust emission standards are being set in many countries. As one of the key technologies, a diesel particulate filter (DPF) for PM trap in the after-treatment of the exhaust gas has been developed. Typically, the inlet size of filter monolith is about 2 mm, and the thickness of the filter wall is only 0.2 mm, where soot particles are removed. It is impossible to observe the small-scale phenomena inside the filter, experimentally. Then, in the present study, we conducted microfluidic simulation with soot oxidation.

Here, a real cordierite filter was used in the simulation. The inner structure of the filter was scanned by a 3D X-ray CT Computed Tomography) technique. The advantage is that it is non-intrusive system, and it has a high spatial resolution in the micrometer. By conducting tomography-assisted simulation, we obtained local velocity and pressure distributions of the complex microfluidics in the filter, which is hardly obtained by measurements. Especially, the conjugate simulation of gas-solid flow was presented. That is, to consider the heat transfer to the solid wall of the filter substrate, the equation of heat conduction was solved, simultaneously. Based on the temperature change and reaction rate in DPF, the conditions for the after-treatment were discussed.

INTRODUCTION

Diesel passenger vehicles have been widely used especially in European countries. Compared with gasoline counterparts, they have good features of high torque at low speed, excellent durability and reliability, higher tolerance to fuel properties, and better fuel efficiency [1]. The main problem with diesel vehicles is that they produce particulate matter (PM) including soot in exhaust gas [2,3]. PM is a serious atmospheric pollutant and is also linked to carcinogenicity [4]. Then, diesel emissions and their control are still very much in the forefront [3,5]. As one of the key technologies, a diesel particulate filter (DPF) for the after-treatment of the exhaust gas has been developed [5, 6, 7]. One example in Fig. 1 is a cordierite filter used in this study. In simple explanation of DPF, it traps PM when exhaust gas passes its porous wall (Fig. 1(b)). It is the most efficient after-treatment device. Latest researches have shown that DPF filtration efficiency can be as high as 99 % [8, 9, 10]. However, the filter would be plugged with diesel soot particles to cause an increase of filter back-pressure, which must be kept at lower levels, because the higher back-pressure increases fuel consumption and reduces available torque [11]. Then, the filter regeneration process with PM oxidation is needed.

Normally, two types of on-board and off-board regenerations are used. As for the off-board regeneration, DPF is periodically replaced, or cleaned to eliminate hydrocarbons and soot particles by an electric heater. The system equipped with a temperature controller, compressed air source, and combustion devices is relatively large and complicated. Thus,

it is more appropriate to use the on-board regeneration, because it is passive regeneration, and its process is spontaneously conducted during the normal engine operation. This process is called continuously regenerating trap [12,13]. However, there is not enough data, and the phenomena occurring in the filter regeneration are not well understood. This is because there are many difficulties in measurements. Typical inlet size of filter monolith is about 2 mm, and the thickness of the filter wall is only 0.2 mm, where soot particles are removed in the after-treatment of diesel exhaust gas. It is impossible to observe the small-scale phenomena inside the filter experimentally.

In this study, we conduct microfluidic simulation of diesel exhaust gas with soot oxidation in the diesel particulate filter. A real cordierite filter is used in the simulation. In the numerical model, the lattice Boltzmann method (LBM) is adopted [14]. In the LBM, the treatment of boundary conditions is simple and easy, and it is appropriate to simulate porous media flow [15, 16, 17]. The inner structure of the filter is scanned by a 3D X-ray CT technique [18, 19, 20, 21]. The advantage is that it is non-intrusive system, and it has a high spatial resolution in the micrometer. By conducting tomography-assisted simulation, we obtain local velocity and pressure distributions of the complex microfluidics in the filter, which is hardly obtained by measurements. Especially, to consider the heat transfer to the solid wall of the filter substrate, the equation of heat conduction is solved, simultaneously. That is, the conjugate simulation of gas-solid flow is presented. Based on the temperature change and reaction rate in DPF, the conditions for the after-treatment are discussed.

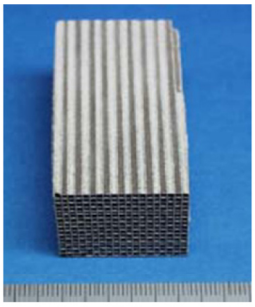

(a)

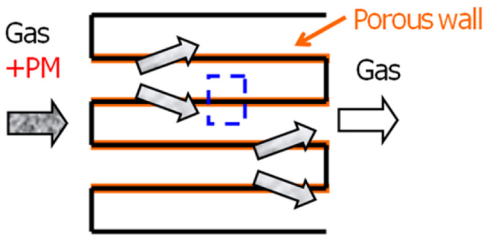

(b)

Figure 1. (a) Photograph of cordierite DPF, and (b) PM trap inside porous filter wall. Calculation domain is shown by dotted line.

NUMERICAL APPROACH

Lattice Boltzmann Method

To simulate the flow in the gas phase, we use the lattice Boltzmann method (LBM). The fundamental idea of LBM is to construct simplified kinetic models that incorporate the essential physics of microscopic or mesoscopic processes so that the macroscopic averaged properties obey the desired macroscopic equations such as the N-S equations. The kinetic equation provides any of the advantages of molecular dynamics, including clear physical pictures, easy implementation of boundary conditions, and fully parallel algorisms [14]. LBM fulfills these requirements in a straightforward manner. So far, many benchmark studies have been conducted [22, 23, 24].

Here, we explain the numerical procedure. The flow is described by the lattice BGK equation in terms of the distribution function. The evolution equation using the pressure distribution function is

$$F_{p,\alpha}(\boldsymbol{x}+\boldsymbol{e}_\alpha\delta_t,\ t+\delta_t)-F_{p,\alpha}(\boldsymbol{x},\ t)=-\frac{1}{\tau_p}[F_{p,\alpha}(\boldsymbol{x},\ t)-F^{eq}_{p,\alpha}(\boldsymbol{x},\ t)] \tag{1}$$

where $c = \delta_x/\delta_t$, and δ_x and δ_t are the lattice constant and the time step, and τ is the relaxation time that controls the rate of approach to equilibrium. The equilibrium distribution function, p_α^{eq}, is given by

$$F^{eq}_{p,\alpha}=w_\alpha\left\{p+p_0\left[3\frac{(\boldsymbol{c}_\alpha\cdot\boldsymbol{u})}{c^2}+\frac{9}{2}\frac{(\boldsymbol{c}_\alpha\cdot\boldsymbol{u})^2}{c^4}-\frac{3}{2}\frac{\boldsymbol{u}\cdot\boldsymbol{u}}{c^2}\right]\right\} \tag{2}$$

The sound speed, c_s, is $c/\sqrt{3}$ with $p_0 = \rho_0 RT_0 = \rho_0 c_s^2$. Here, p_0 and ρ_0 are the pressure and density in the reference conditions. In this study, to consider the variable density, we adopt the low Mach number approximation [22, 23, 24]. 3D simulation is conducted by D3Q15 model. Then, the pressure drop across the filter is simulated more precisely. To validate our numerical scheme, we compare numerical results with an empirical equation in porous media theory [25].

The pressure and local velocity of $\boldsymbol{u}=(u_x, u_y, u_z)$ are obtained using the ideal gas equation.

$$p=\sum_\alpha F_{p,\alpha} \tag{3}$$

$$\boldsymbol{u}=\frac{\rho_0}{\rho}\frac{1}{p_0}\sum_\alpha \boldsymbol{c}_\alpha F_{p,\alpha} \tag{4}$$

The relaxation time is related with transport coefficients such as kinetic viscosity using $\nu = (2\tau_p - 1)/6\ c^2\ \delta_t$. Through the

Chapman-Enskog procedure, the Navier-Stokes equations are derived from these equations [14]. The LBM formula for temperature and concentration fields is

$$F_{s\alpha}(\boldsymbol{x}+\boldsymbol{c}_\alpha\delta_t,\ t+\delta_t)-F_{s\alpha}(\boldsymbol{x},\ t)=-\frac{1}{\tau_s}[F_{s\alpha}(\boldsymbol{x},\ t)-F_{s\alpha}^{eq}(\boldsymbol{x},\ t)]+w_\alpha Q_s,$$
$$s=T,\ Y_i \qquad (5)$$

where Q_S is the source term due to chemical reaction. The equilibrium distribution function, $F_{S,\alpha}^{eq}$, is

$$F_{s,\alpha}^{eq}=w_\alpha\cdot s\left\{1+3\frac{(\boldsymbol{c}_\alpha\cdot\boldsymbol{u})}{c^2}+\frac{9}{2}\frac{(\boldsymbol{c}_\alpha\cdot\boldsymbol{u})^2}{c^4}-\frac{3}{2}\frac{\boldsymbol{u}^2}{c^2}\right\} \qquad (6)$$

Temperature, T, and mass fraction of species, Y_i, are determined by these distribution functions.

$$T=\sum_\alpha F_{T,\alpha} \qquad (7)$$

$$Y_i=\sum_\alpha F_{Yi,\alpha} \qquad (8)$$

Heat Transfer in Solid Phase

In the soot oxidation process, the gas phase temperature due to soot combustion becomes high to cause the heat transfer to the solid phase of the filter substrate. Then, the following equation of heat conduction is solved.

$$\frac{\partial T}{\partial t}=\frac{\lambda}{\rho_s C_p}\left\{\frac{\partial^2 T}{\partial x^2}+\frac{\partial^2 T}{\partial y^2}+\frac{\partial^2 T}{\partial z^2}\right\} \qquad (9)$$

where λ, ρ_s and C_p are the heat conductivity, density, and heat capacity of the filter. These values of the cordierite filter are 1.9 W/mK, 2500 kg/m^3, and 1170 J/kgK [26]. The convection and chemical reaction are not included in this equation. By coupling the equations in gas phase and using appropriate boundary conditions, it is possible to solve the conservation equations of gas and solid phases. In order to determine the temperature at the interface between two phases, it is assumed that the temperature and heat flux in the gas phase are equal to those in solid phase. Other boundary conditions are explained in the next section.

Calculation Domain and X-Ray CT Technique

To simulate the flow in the real diesel filter, we obtain the inner structure by the 3D X-ray CT (Computed Tomography) technique. Non-destructive nature of the CT technique allows visualization of filter inner structure actually used. We have confirmed the applicability of the tomography-assisted simulation [18, 19, 20, 21]. In the present study, we employ a similar data processing technique.

Figure 2 shows structure of DPF obtained by X-ray CT technique. Upper figure shows a CT image of the filter, and lower figure shows a 3D reconstructed image data used in the simulation. The spatial resolution is 1 μm/pixel, which is the finest level in the reported CT measurements. The image area is 400 μm (x) × 400 μm (y) × 200 μm (z). The exhaust gas passes through the filter wall in the x-direction. Complex porous structure with variety of pore size is well observed. The averaged porosity of the filter, ε, is about 0.4. In the simulation of flow with the soot oxidation process, a part of CT data is used.

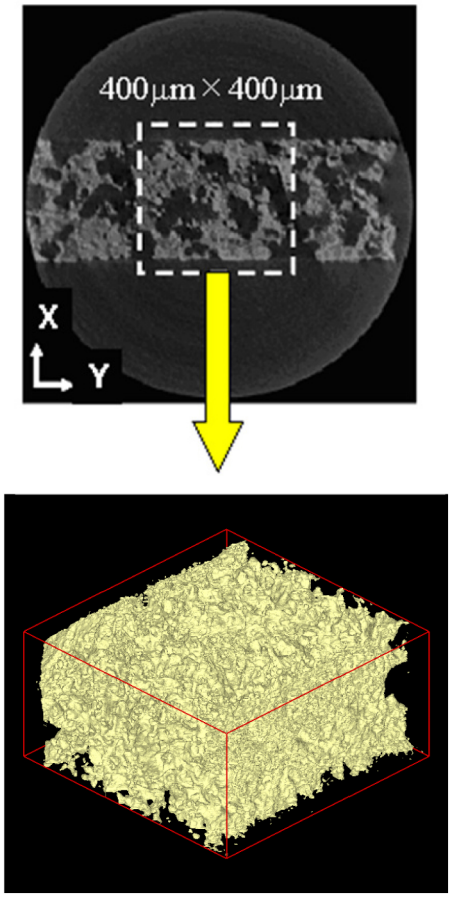

Figure 2. Structure of DPF obtained by X-ray CT technique. Upper figure shows a CT image of the filter, and lower figure shows a 3D reconstructed image data used in the simulation.

Figure 3 shows the 3D calculation domain. Its size is 400 μm × 40 μm × 40 μm, and the grid number is 401 (N_x)× 41 (N_y) ×41 (N_z). The grid size is 1 μm, which is the spatial resolution in X-ray CT measurement. For the sot oxidation process, an over-all reaction by Lee et al. [27] is used. For simplicity, any catalytic effects are not considered.

As for the boundary condition, the inflow boundary is adopted at the inlet [28]. The inlet velocity of U_{in} is varied from 0.1 to 20 m/s, and the oxygen concentration of exhaust

gas is changed. The gas component is of the diesel exhaust gas, and its temperature is 673 K [18,20]. The soot mass fraction is also varied from 0.01 to 0.04. At the sidewall, the slip boundary conditions are adopted, considering the symmetry [29]. At the outlet, the pressure is constant, and the gradient of scalar such as temperature and mass fraction is set to be zero. On the surface of the filter substrate, the non-slip boundary condition is adopted [30].

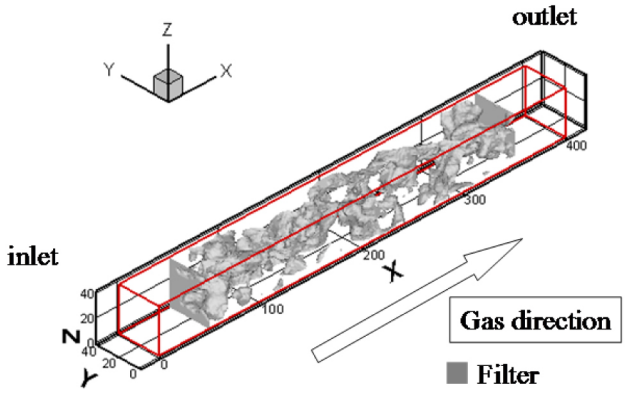

Figure 3. Numerical domain and coordinate.

RESULTS AND DISCUSSION

Flow Inside DPF

Before simulating the after-treatment of exhaust gas, we examine the flow inside the filter. The cold flow at room temperature is used. Figure 4 shows the velocity field with velocity vector. The flow is under steady state with small velocity perturbation. The inlet velocity is 1 m/s. The velocity vector is shown, with filter substrate by gray region. It is found that the ceramic filter has many small pores. Then, the velocity and its direction are largely changed when the flow passes through the filter wall.

To confirm the validity of numerical scheme, simulation results are compared with the empirical equation. The idea is based on the porous media flow theory [25]. First, the hydraulic radius, R_h, and the equivalent diameter of the filter substrate, D_p are determined.

$$R_h = \frac{volume\ available\ for\ flow}{total\ wetted\ surface} \tag{10}$$

$$D_p = 6R_h \frac{1-\varepsilon}{\varepsilon} \tag{11}$$

The friction factor, f, and Reynolds number, Re, are defined by

$$f = \left(-\frac{dp}{dx}\right)\frac{D_p}{\rho_0 U_{in}^2}\frac{\varepsilon^3}{(1-\varepsilon)} \tag{12}$$

$$\mathrm{Re} = \frac{U_{in} D_p}{\nu(1-\varepsilon)} \tag{13}$$

The empirical equation, which is called an Ergun equation, is as follows:

$$f = 150/\mathrm{Re} + 1.75 \tag{14}$$

Here, we conduct a grid convergent study to confirm the proper calculation domain in tomography-assisted simulation. The following four cases are considered.

Case 1. 400 μm (x) × 40 μm (y) × 40 μm (z)

Case 2. 400 μm (x) × 60 μm (y) × 60 μm (z)

Case 3. 400 μm (x) × 80 μm (y) × 80 μm (z)

Case 4. 400 μm (x) × 100 μm (y) × 100 μm (z)

Figure 5 shows simulation results, compared with the empirical equation. For all cases, a good agreement with empirical equation is observed. Although the computational domain is limited in our tomography-assisted simulation, it is confirmed that we could discuss the heat and mass transfer in the real filter.

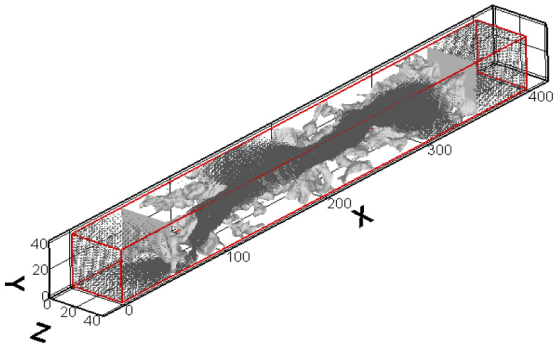

Figure 4. Flow field inside DPF with velocity vector.

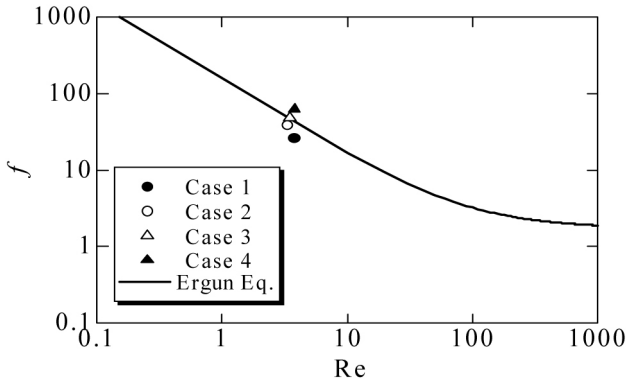

Figure 5. Variations of friction factor with Reynolds number.

Soot Oxidation for After-Treatment of Exhaust Gas

Next, the soot oxidation process is considered to simulate the after-treatment of exhaust gas. Initially, there is no soot in DPF, considering the clean filter. Since the soot and oxygen are included in the inflow gas, the soot is automatically oxidized if the temperature is high enough. To initiate the reaction in the filter, the wall of the filter substrate is set to be 1200 K. The mass fraction of soot is 0.05, and the temperature of inflow gas is changed. The oxygen volumetric concentration is 10 or 20%, and the inflow velocity is 1 m/s.

First, the temperature field is examined to observe the heat transfer inside the filter. Figure 6 shows the time variation of temperature profile. Time, t, is counted after we start the simulation. The temperature of inflow gas is 400 °C (673 K), and the oxygen volumetric concentration is 10%. It is found that, at the beginning, only the temperature of gas phase is increased due to the soot oxidation. Then, the filter substrate of solid phase is heated. The simulation is continued until the steady state is achieved.

Then, the soot oxidation process is investigated. The conditions are the same. Figure 7 shows the distributions of flow field with velocity vector, soot mass fraction in gas phase, and temperature. The steady state is achieved at t = 0.5s. Exhaust gas passes through the tunnel in pores inside the DPF, and the complex flow pattern is observed. The temperature of gas phase as well as that of solid phase is almost uniform. As seen in Fig.7(b), the soot concentration is decreased by the reaction with oxygen. The reaction rate near the inlet is larger, because the soot concentration as well as the oxygen concentration is high. The reaction rate locally varies, simply because the mass transfers of these reactants are different. At the filter exit, the soot concentration is not zero, and a part of soot is not oxidized inside the filter. That is, the after-treatment process is not completed at this condition.

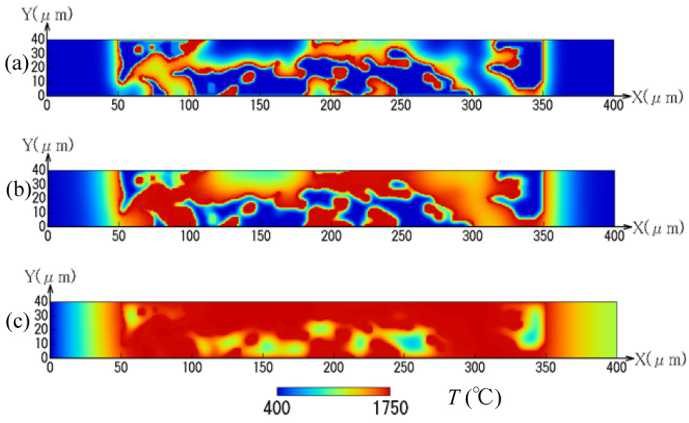

Figure 6. Time variation of temperature profile; (a) t =0.3 ms, (b) t =2 ms, (c) t = 20 ms

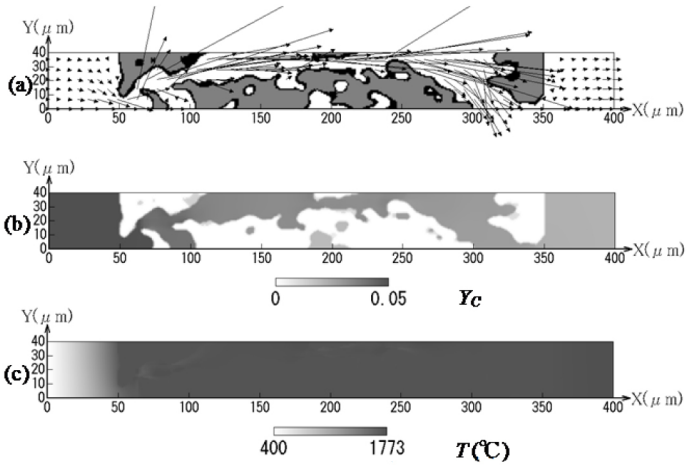

Figure 7. Distributions of (a) flow field with velocity vector, (b) soot mass fraction in gas phase, (c) temperature

For further discussion, the temperature of exhaust gas is changed. Figure 8 shows the soot mass fraction along the flow direction of x. Two different inlet temperatures of T_{in} are considered, which are 400 and 700 °C. The soot mass fraction at the inlet is 0.05, and the oxygen volumetric concentration is 10%. To evaluate the degree of soot oxidation, the soot mass fraction at any coordinate is divided by the value at the inlet. Then, it is possible to check the degree of soot oxidation. It is found that these profiles are quite similar. Expectedly, the soot mass fraction at higher inlet temperature is smaller, because more soot is oxidized.

Next, the oxygen concentration is changed, which could be an important parameter to control the soot oxidation rate [31,32]. Results are shown in Fig. 9. Two cases are considered. The oxygen volumetric concentration of X_{O2} is 10% and 21%. The inlet temperatures is 400 °C, and the soot mass fraction at the inlet is 0.05. Needless to say, it is seen that more soot is oxidized at higher oxygen concentration. Then, the soot oxidation process is promoted by increasing the oxygen concentration.

Here, we monitor the soot mass fraction at the filter exit by changing the oxygen concentration. The inlet temperatures are 400 and 700 °C. Results are shown in Fig. 10. In the simulation, the oxygen volumetric concentration is varied from 10 to 21%. The soot mass fraction at the inlet is 0.05. Two inlet temperatures are considered. When the oxygen concentration in exhaust gas is small, a part of soot is not oxidized inside the filter, because the temperature is not high enough to achieve the complete after-treatment. However, when more oxygen is included in the exhaust gas, the temperature inside DPF becomes higher to intensify the soot oxidation process. When the oxygen concentration is over 20% at T_{in} = 700 °C, the soot concentration at the filter exit is completely zero. This inlet temperature could be relatively higher, because any catalysts are not considered in this study.

In future study, the numerical simulation of the catalyzed DPF will be conducted [33].

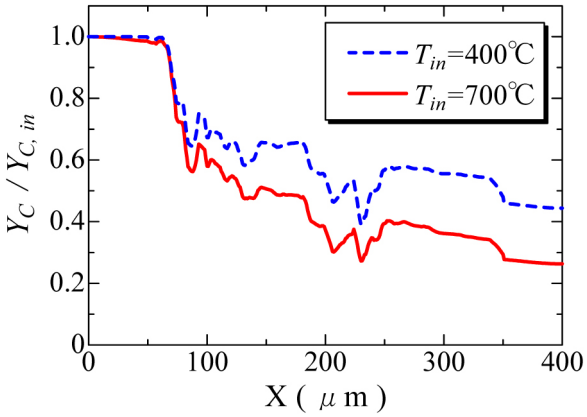

Figure 8. Distribution of soot mass fraction in gas phase at different inlet temperature.

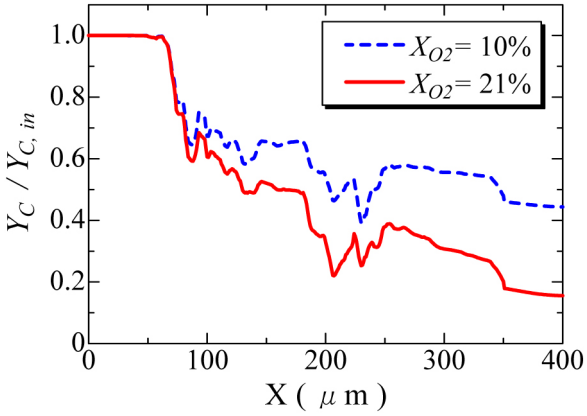

Figure 9. Distribution of soot mass fraction in gas phase at different oxygen concentration of exhaust gas.

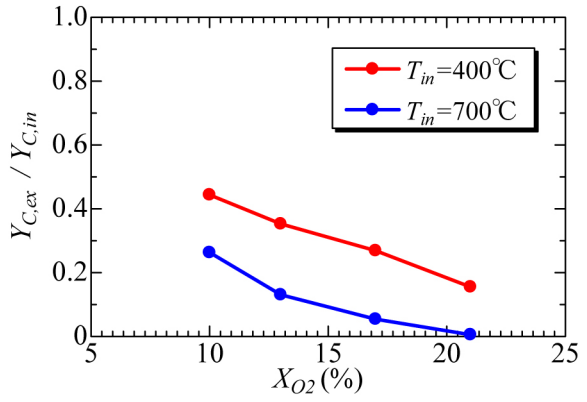

Figure 10. Variations of soot mass fraction at exit with oxygen concentration of exhaust gas.

CONCLUSIONS

By conducting microfluidic simulation of diesel exhaust gas, we discussed the soot oxidation phenomena in the aftertreatment of diesel exhaust gas. The following results were obtained:

(1). Even in cold flow, the complex flow pattern is observed due to the non-uniformity of pore structure inside the filter. Although the calculation domain is limited, the simulation results show a good agreement with empirical equation of the Ergun equation.

(2). Based on the profiles of soot concentration and soot oxidation rate, we could discuss the heat and mass transfer in the after-treatment process. When the soot concentration in exhaust gas is small, a part of soot is not oxidized inside the filter, because the temperature is not high enough to achieve the complete oxidation of diesel soot.

(3). When the inlet temperature of exhaust gas is higher, more soot is oxidized inside DPF. The soot consumption rate (soot oxidation rate) is balanced with the soot supply in the inflow of exhaust gas. As the oxygen concentration is higher, the soot oxidation rate becomes higher, showing that the exhaust oxygen concentration is an important parameter to promote the after-treatment process inside the filter.

REFERENCES

1. Yezerets, A., Currier, N. W., Kim, D.H., Eadler, H.A., Epling, W.S., Peden, C.H.F., "Differential Kinetic Analysis of Diesel Particulate Matter (Soot) Oxidation by Oxygen Using a Step-Response Technique," Applied Catalysis B 61 (2005) 120-129.

2. Kittelson, D.B., "Engines and Nanoparticles: A Review," Journal of Aerosol Science 29 (1998), 575-588.

3. Johnson, T., "Review of Diesel Emissions and Control," *SAE Int. J. Fuels Lubr.* 3(1):16-29, 2010, doi: 10.4271/2010-01-0301.

4. Kennedy, I. M., "The Health Effects of Combustion-Generated Aerosols", Proc. Combust. Inst. 31 (2007) 2757-2770.

5. Tzamkiozis, T., Ntziachristos, L., Samaras, Z., "Diesel Passenger Car PM Emissions: From Euro 1 to Euro 4 with Particle Filter," Atmospheric Environment 44 (2010), 909-916.

6. Koltsakis, G.C., Stamatelos, A.M., "Catalytic Automotive Exhaust After-Treatment," Prog. Energy Combust. Sci. 23 (1997) 1-39.

7. Adler, J., "Ceramic Diesel Particulate Filters," International Journal of Applied Ceramic Technology 2 (2005), 429-439.

8. Clerc, J.C., "Catalytic Diesel Exhaust Aftertreatment," Applied Catalysis B 10 (1996) 99-115.

9. Konstandopoulos, A., Kostoglou, M., Skaperdas, E., Papaioannou, E. et al., "Fundamental Studies of Diesel Particulate Filters: Transient Loading, Regeneration and Aging," SAE Technical Paper 2000-01-1016, 2000, doi: 10.4271/2000-01-1016.

10. Wirojsakunchai, E., Schroeder, E., Kolodziej, C., Foster, D. et al., "Detailed Diesel Exhaust Particulate Characterization and Real-Time DPF Filtration Efficiency Measurements During PM Filling Process," SAE Technical Paper 2007-01-0320, 2007, doi: 10.4271/2007-01-0320.

11. Stamatelos, A.M., "A Review of the Effect of Particulate Traps on the Efficiency of Vehicle Diesel Engines," Energy Conversion and Management, Vol.38(1) (1997) 83-99.

12. Cooper, B.J., Jung, H.J., and Toss, J.E. (1990), US Patent, 4902487.

13. Hawker, P. (1995) "Diesel emission control technology," Platinum Metals Rev., Vol. 39, pp.2-8.

14. Chen S., and Doolen, G.D., "Lattice Boltzmann Method for Fluid Flows," Annual Review of Fluid Mechanics, Vol. 30, pp.329-364, 1998.

15. Cancelliere, A., Chang, C., Foti, E., Rothman, D.H., Succi, S., "The Permeability of a Random Medium: Comparison of Simulation with Theory", Phys. Fluids A, Vol.2, pp.2085-2088, 1990.

16. Inamuro, T., Yoshino, M., Ogino, F., "Lattice Boltzmann Simulation of Flows in a Three-dimensional Porous Structure.", Int. J. Numer. Methods Fluids, Vol.29, pp. 737-748, 1999.

17. Bernsdorf, J., Brenner, G., Durst, F., "Numerical Analysis of the Pressure Drop in Porous Media Flow with the Lattice Boltzmann (BGK) Automata", Comput. Phys. Commun., Vol.129, pp.247-255, 2000.

18. Yamamoto, K., Oohori, S., Yamashita, H., Daido, S., "Simulation on Soot Deposition and Combustion in Diesel Particulate Filter," Proceedings of the Combustion Institute, Vol.32, pp.1965-1972, 2009.

19. Yamamoto, K., Satake, S., Yamashita, H., Takada, N., Misawa, M., "Fluid Simulation and X-ray CT Images for Soot Deposition in a Diesel Filter", the European Physical Journal, Vol.171, pp.205-212, 2009.

20. Yamamoto, K., Nakamura, M., Yane, H., Yamashita, H., "Simulation on Catalytic Reaction in Diesel Particulate Filter," Catalysis Today, Vol.153, pp.118-124, 2010.

21. Yamamoto, K., Yamauchi, K., Takada, N., Misawa, M., Furutani, H., Shinozaki, O., "Lattice Boltzmann Simulation on Continuously Regenerating Diesel Filter," Philosophical Transactions A (The Royal Society, London), Vol.369, 2584-2591, 2011.

22. Yamamoto, K., He, X., and Doolen, G.D. "Simulation of Combustion Field with Lattice Boltzmann Method," Journal of Statistical Physics, Vol. 107(1/2), pp.367-383, 2002.

23. Yamamoto, K., "LB simulation on combustion with turbulence," International Journal of Modern Physics B, Vol. 17(1/2), pp.197-200, 2003.

24. Yamamoto, K., He, X., and Doolen, G.D., "Combustion Simulation Using the Lattice Boltzmann Method," JSME International Journal, Series B, Vol. 47(2), pp.403-409, 2004.

25. Bird, R.B., Stewart, W.E. and Lightfoot, E.N., Transport Phenomena, Wiley, New York, 1960.

26. Yamamoto, K., Nakamura, M., "Conjugate Simulation of Flow and Heat Transfer in Diesel Particulate Filter," Progress in Computational Fluid Dynamics (PCFD), Vol.12, No.4, 286-292, 2012.

27. Lee, K.B., Thring, M.W., and Beer. J.M., "On the Rate of Combustion of Soot in a Laminar Soot Flame,", Comb. Flame, Vol. 6, pp.137-145, 1962.

28. He, X., Chen, S., and Doolen, G.D., "A Novel Thermal Model for the Lattice Boltzmann Method in Incompressible Limit," J. Comp. Phys., Vol. 146, No. 1, pp.282-300, 1998.

29. Inamuro, T., Yoshino, M., and Ogino, F., "Lattice Boltzmann Simulation of Flows in a Three-Dimensional Porous Structure," Int. J. Numer. Meth. Fluids, Vol. 29, pp. 737-748, 1999.

30. He, X., and Luo, Li-Shi, "Lattice Boltzmann Model for the Incompressible Navier-Stokes Equation," Journal of Statistical Physics, 88(3/4), pp.927-944, 1997.

31. Pattas, K., Stamatelos, A., Kougianos, K., Koltsakis, G. et al., "Trap Protection by Limiting A/F Ratio During Regeneration," SAE Technical Paper 950366, 1995, doi: 10.4271/950366.

32. Tsuneyoshi, K., Takagi, O., and Yamamoto, K., "Effects of Washcoat on Initial PM Filtration Efficiency and Pressure Drop in SiC DPF," SAE Technical Paper 2011-01-0817, 2011, doi: 10.4271/2011-01-0817.

33. Yamamoto, K., Yamauchi, K., "Numerical Simulation of Continuously Regenerating Diesel Particulate Filter," Proceedings of the Combustion Institute, Vol.34, pp. 3083-3090, 2013, doi: 10.1016/j.proci.2012.06.117.

CONTACT INFORMATION

Corresponding Author:

Kazuhiro Yamamoto
kazuhiro@mech.nagoya-u.ac.jp

ACKNOWLEDGMENTS

This work was partially supported by the Rare Metal Substitute Materials Development Project of New Energy and Industry Technology Development Organization (NEDO) in Japan.

DEFINITIONS

$\boldsymbol{c}$ - Advection speed in LB coordinate

$\boldsymbol{C_p}$ - Heat capacity of filter

$\boldsymbol{c_s}$ - Sound speed

$\boldsymbol{D_p}$ - Equivalent diameter

$\boldsymbol{f}$ - Friction factor

$\boldsymbol{F_{p,\alpha}}$ - Distribution function of pressure

$\boldsymbol{F_{s,\alpha}}$ - Distribution function of temperature or species concentration

$\boldsymbol{p}$ - Pressure

$\boldsymbol{Q_s}$ - Source term by chemical reaction

$\boldsymbol{R}$ - Ideal gas constant

Re - Reynolds number

$\boldsymbol{R_h}$ - Hydraulic radius

$\boldsymbol{s}$ - Scalar of temperature or species concentration

$\boldsymbol{t}$ - Time

$\boldsymbol{T}$ - Temperature

$\boldsymbol{u}$ - Velocity vector

$\boldsymbol{U_{in}}$ - Inlet velocity

$\boldsymbol{X_i}$ - Mole fraction of species i

$\boldsymbol{x}$ - Coordinates of (x, y, z)

$\boldsymbol{x}$ - Direction normal to the filter wall

$\boldsymbol{y}$ - Direction normal to x

$\boldsymbol{z}$ - Direction normal to x

$\boldsymbol{Y_i}$ - Mass fraction of species i

$\boldsymbol{\varepsilon}$ - Porosity

$\boldsymbol{\lambda}$ - Heat conductivity of filter substrate

$\boldsymbol{\nu}$ - Kinetic viscosity

$\boldsymbol{\rho}$ - Density of mixture

$\boldsymbol{\tau}$ - Relaxation time

Subscript

0 - Reference condition

C - Properties of soot

exit - Value at exit

in - Value at inlet

s - Properties of filter substrate

$\boldsymbol{\alpha}$ - Number of advection speed in LB coordinate

The Engineering Meetings Board has approved this paper for publication. It has successfully completed SAE's peer review process under the supervision of the session organizer. This process requires a minimum of three (3) reviews by industry experts.

ISSN 0148-7191

SAE Customer Service:
Tel: 877-606-7323 (inside USA and Canada)
Tel: 724-776-4970 (outside USA)
Fax: 724-776-0790
Email: CustomerService@sae.org
SAE Web Address: http://www.sae.org
Printed in USA